GMR
The Original

SUSTAINABLE GREEN FABRICATION OF STARCH/PVA/CUO ELECTROSPUN NANOFIBERS FROM *ECTOCARPALES* (BROWN MARINE MACROALGAE) EXTRACT: PHYSICOCHEMICAL CHARACTERIZATION AND ANTICANCER POTENTIAL ON HT-29 AND MCF-7 CELLS

Vinuritha Kandaswamy[1], Sangamithra C[2], Alagendran Subbarayalu[3]*

[1]Saveetha Medical College & Hospital (SMCH), Saveetha Institute of Medical and Technical Sciences (SIMATS), Thandalam, Chennai, Tamil Nadu 602105, India. vinu.kandha5@gmail.com
[2]Department of Anesthesiology, Saveetha Medical College and Hospital, Saveetha Institute of Medical And Technical Sciences (SIMATS), Thandalam, Chennai-602105, Tamil Nadu, India. Email: sangmichandru@gmail.com; ORCID: https://orcid.org/0009-0004-1601-8640.
[3]Clinical Neuroscience and Phytomedicine Laboratory, Department of Research, Saveetha College of Nursing (SCON), Saveetha Institute of Medical and Technical Sciences (SIMATS), Chennai 602105, Tamil Nadu, India. Email: proteinblg@gmail.com; alagendrans.scon@saveetha.com. ORCID: https://orcid.org/0009-0009-0749-7180.
*Correspondence: proteinblg@gmail.com; alagendrans.scon@saveetha.com (A.S.)

ABSTRACT
This research presents the green synthesis of copper oxide nanoparticles (CuO NPs) using *Ectocarpales* marine algae extract and their integration into starch/polyvinyl alcohol (PVA) nanoscaffolds. The synthesized CuO NPs and nanoscaffolds were characterized using UV-Visible spectroscopy, Fourier-transform infrared spectroscopy (FTIR), X-ray diffraction (XRD), Scanning electron microscopy (SEM), Thermogravimetric analysis (TGA), and Dynamic light scattering (DLS), confirming successful nanoparticle formation, crystalline structure, and uniform dispersion within the polymer matrix. The nanoscaffolds exhibited enhanced thermal stability and a porous fibrous morphology, ideal for biomedical applications. Anticancer activity was evaluated against HT-29 and MCF-7 cell lines, showing dose-dependent cytotoxicity. Notably, the starch/PVA/CuO-NPs nanoscaffolds demonstrated significantly higher anticancer efficacy with lower IC_{50} values compared to CuO NPs and algal extract alone. These results highlight the synergistic potential of combining biogenic CuO NPs with biodegradable polymer scaffolds for targeted cancer therapy. This study underscores the promise of such nanocomposites as advanced therapeutic platforms, warranting further investigation into their mechanisms and *in vivo* performance.

KEYWORDS: *Ectocarpales*, Green synthesis, CuO nanoparticles, Starch/PVA/CuO-NPs nanoscaffolds, Anticancer activity.

1. INTRODUCTION

Cancer remains one of the most significant public health concerns worldwide, accounting for nearly 10 million deaths annually, as per the World Health Organization. Despite the availability of conventional treatments like chemotherapy, radiation, and surgery, their non-specific nature often causes severe side effects, toxicity to healthy tissues, and the development of multidrug resistance [1]. These limitations necessitate the development of alternative therapeutic strategies that are both biocompatible and effective in selectively targeting cancer cells [2]. In this context, nanotechnology-based drug delivery systems and scaffolds have gained considerable attention due to their ability to enhance drug bioavailability, improve targeting, and reduce systemic toxicity [3].

Among the various types of nanomaterials explored, metal oxide nanoparticles—particularly copper oxide nanoparticles (CuO NPs)—have emerged as promising agents in cancer therapy [4]. CuO NPs possess unique properties such as large surface area-to-volume ratio, high catalytic efficiency, and the ability to generate reactive oxygen species (ROS), which contribute to their cytotoxic activity against cancer cells [5]. Unlike traditional cytotoxic agents, CuO NPs exhibit selective toxicity by inducing oxidative stress within tumor environments, ultimately triggering apoptosis [6]. However, the synthesis of CuO NPs through conventional chemical methods often involves hazardous solvents and high energy inputs, posing environmental and biological safety concerns [5].

To address these issues, green synthesis of nanoparticles using biological resources has become an appealing alternative [7]. Marine macroalgae, especially brown algae of the order *Ectocarpales*, offer a sustainable and eco-friendly route for nanoparticle synthesis [8]. These algae are rich in polysaccharides, polyphenols, and other phytoconstituents that act as natural reducing and stabilizing agents [9]. Furthermore, the unique bioactive profile of marine algae contributes additional therapeutic benefits, including anti-inflammatory, antioxidant, and

anticancer properties [10]. Ultrasound-assisted extraction techniques further improve the release of these bioactive compounds by enhancing cell wall disruption and increasing extraction efficiency, resulting in a potent extract that can facilitate the biogenic synthesis of nanoparticles [11].

Parallel to the development of nanotherapeutics, biomaterial-based scaffolds have emerged as crucial platforms for controlled drug delivery, tissue engineering, and cancer therapy [12]. Electrospun nanofibers, in particular, are gaining popularity due to their high porosity, large surface area, and ability to mimic the extracellular matrix (ECM) [13]. These characteristics make them suitable for incorporating and releasing therapeutic agents in a sustained manner [14]. Among various polymers explored for scaffold fabrication, starch and polyvinyl alcohol (PVA) have shown significant promise [15]. Starch is a naturally derived, biodegradable, and biocompatible polysaccharide, whereas PVA is a synthetic polymer known for its flexibility, hydrophilicity, and electrospinnability [16]. When blended, starch and PVA create a hybrid matrix with improved mechanical strength and biofunctional properties [17].

Incorporating CuO NPs synthesized from marine algal extracts into starch/PVA electrospun nanofibers provides a novel and synergistic strategy for cancer treatment [18]. This hybrid system combines the structural advantages of electrospun fibers with the therapeutic efficacy of both the marine-derived phytoconstituents and CuO NPs [19]. Furthermore, the electrospinning process facilitates the encapsulation of nanoparticles in a uniform, fibrous matrix, enabling sustained and localized drug delivery at the tumor site [20]. The resulting nanofibrous scaffold not only functions as a delivery system but also exhibits intrinsic anticancer activity through multiple mechanisms, including oxidative stress induction, DNA damage, and mitochondrial dysfunction [21].

The present study focuses on the ultrasound-assisted green synthesis of CuO NPs using *Ectocarpales* brown algae extract and their incorporation into starch/PVA-based electrospun nanofibers. The synthesized CuO NPs were characterized using various spectroscopic and microscopic techniques to confirm their structural integrity, morphology, and stability [22]. The starch/PVA/CuO hybrid nanofibers were fabricated under optimized electrospinning parameters and characterized for their physicochemical properties, including thermal stability, surface morphology, functional group distribution, and crystallinity [23].

In vitro cytotoxicity was evaluated using two human cancer cell lines: HT-29 (colon carcinoma) and MCF-7 (breast adenocarcinoma), to determine the anticancer efficacy of the algal extract, CuO NPs, and CuO-incorporated nanofibers [24]. The MTT assay was employed to quantify cell viability post-treatment and assess dose-dependent cytotoxic effects [25]. The study also employed statistical analyses to validate the significance of observed effects and correlations [26].

Overall, this research integrates the fields of green nanotechnology, marine pharmacognosy, and electrospun biomaterials to create a novel biofunctional platform for cancer therapy [27]. By harnessing the ecological sustainability of marine algae, the therapeutic potential of CuO NPs, and the delivery capabilities of starch/PVA nanofibers, the study aims to pave the way for the development of biocompatible and eco-friendly anticancer materials [28]. The successful demonstration of this strategy could lead to the design of next-generation scaffolds with tunable properties for various biomedical applications, particularly in localized cancer treatment [29].

2. MATERIALS AND METHODS

2.1. Chemicals and materials

Marine brown algae belonging to the *Ectocarpales* order were collected from the coastal region of Rameswaram, Tamil Nadu, and served as a sustainable biosource for synthesizing CuO NPs via green synthesis. Copper (II) sulfate pentahydrate ($CuSO_4 \cdot 5H_2O$, Sigma-Aldrich) functioned as the precursor salt. PVA, with an average molecular weight of 145,000, and commercially available starch were utilized for creating electrospun nanofiber mats using a HOLMARC HO-NFES-040 electrospinning unit. All other solvents and reagents, purchased from Sigma-Aldrich and Merck, were of analytical grade and used without any further processing. Analytical techniques included UV-visible spectroscopy, Fourier-transform infrared spectroscopy (FTIR), X-ray diffraction (XRD) using a Bruker D8 Advance, Scanning electron microscopy (SEM) via JEOL JSM-IT800, zeta potential via Malvern Zetasizer Ultra, and thermal analysis using PerkinElmer Thermogravimetric analysis (TGA) 8000. Anticancer effects were assessed using standard evaluation protocols.

2.2. Collection and preparation of *Ectocarpales* algae

Brown algae of the *Ectocarpales* group were manually gathered from the intertidal zone along the Rameswaram coast. To eliminate physical contaminants, samples were initially washed with tap water to remove sand and debris, then rinsed with distilled water for further purification. Approximately 100 g of cleaned algae were chopped into small fragments and subjected to shade drying at ambient temperature (~28°C) for 14 days. The dried algal material was ground into a fine powder using a mechanical grinder and stored in moisture-free airtight containers for subsequent use.

2.3. Ultrasound-assisted extraction of bioactive compounds

To extract phytochemicals, 2 g of algal powder was suspended in 50 mL of Milli-Q water in a sterilized beaker. This mixture was placed in a LABQUEST ultrasonic bath (Borosil; Serial No. 941032329018) at 60°C for 45 minutes. Ultrasonication disrupted algal cell walls, enhancing the release of bioactive components. The solution was then filtered using Whatman No. 1 paper under sterile conditions. The resulting filtrate was either stored at 10°C for immediate use or freeze-dried to obtain a stable powdered extract for future applications [30, 31].

2.4. Green synthesis of CuO NPs

The algal extract served as a reducing and stabilizing agent for synthesizing CuO NPs. A 0.1 M aqueous $CuSO_4 \cdot 5H_2O$ solution (50 mL) was combined with 10 mL of extract (10 mg lyophilized powder in 10 mL Milli-Q water) in a 5:1 ratio. The mixture was stirred magnetically at 650 rpm and maintained at 60°C for 2 hours. Formation of nanoparticles was indicated by a color change from deep blue to bluish-green. The resulting solution was washed three times with double-distilled water to eliminate residual biomolecules and salts. Lyophilization for 48 hours yielded a fine CuO nanopowder for downstream applications [32].

2.5. Fabrication of starch/PVA nanofibers embedded with CuO NPs

To fabricate hybrid nanofibers, 15% (w/w) PVA was dissolved in distilled water under consistent heat and stirring. Once fully solubilized, 100 mg each of starch and synthesized CuO NPs were added and stirred at 50°C for 2.5 hours to ensure even dispersion. The polymer blend was transferred to a syringe equipped with a 0.84 mm needle and electrospun using a HOLMARC HO-NFES-040 system. The optimized conditions included an applied voltage of 11.5 kV, a nozzle-to-collector gap of 12.3 cm, and a flow rate of 0.4 mL/h. The nanofibers were collected on aluminum foil for 6–8 hours at ambient temperature, forming uniform fibrous mats [33-35].

2.6. Physicochemical characterization methods

2.6.1. UV-visible spectral analysis

A VIS SPEC V-730 spectrophotometer was used to determine the optical absorption characteristics of algal extract, CuO NPs, and composite nanofibers. Absorbance spectra were recorded from 200 to 800 nm, using deionized water as the blank reference [36].

2.6.2. FTIR spectroscopic analysis

FT-IR spectra were acquired using a PerkinElmer Spectrum Two spectrometer in ATR mode, over a wavenumber range of 4000–400 cm^{-1}. The resolution was set at 4 cm^{-1}, and each spectrum was averaged over 64 scans to improve signal clarity and identify functional groups related to synthesis and scaffold structure [37].

2.6.3. XRD analysis

XRD was conducted on a Bruker D8 Advance diffractometer using CuKα radiation (λ = 1.5406 Å), operated at 40 kV and 40 mA. Data acquisition ranged from 2θ = 5° to 90° at a scan step size of 0.029649°, revealing crystalline structures within nanoparticles and composites [38].

2.6.4. SEM analysis

Surface morphology of CuO NPs and nanofiber mats was examined via a JEOL JSM-IT800 SEM. Prior to imaging, samples were gold-coated to enhance conductivity and resolution. SEM was used to analyze fiber uniformity, particle dispersion, and topographical features [39].

2.6.5. TGA

Thermal properties were evaluated using a PerkinElmer TGA 8000. Around 5 mg of each sample was heated from room temperature to 550°C at a rate of 15°C/min under a nitrogen atmosphere. Thermal stability and decomposition patterns were recorded [40].

2.6.6. Particle size and zeta potential analysis

A Malvern Zetasizer Ultra was employed to assess the hydrodynamic diameter and zeta potential of CuO NPs using dynamic and electrophoretic light scattering. These parameters provided insight into colloidal stability and particle dispersion [41].

All physicochemical data are available at Mendeley Data (DOI: 10.17632/m7jzmb7mr9.1).

2.7. *In vitro* anticancer activity

2.7.1. Procurement and culture of HT-29 and MCF-7 cells

Human cancer cell lines, HT-29 (colon) and MCF-7 (breast), were sourced from the National Center for Cell Science (NCCS), Pune, India. Cells were cultured in Minimum Essential Medium (MEM) supplemented with 10% fetal bovine serum (FBS) at 37°C in a humidified 5% CO_2 incubator [24].

2.7.2. MTT cell viability assay

To assess cytotoxicity, HT-29 and MCF-7 cells were seeded in 96-well plates at a density of 5×10^5 cells per well and allowed to adhere overnight. Cells were then treated with varying concentrations (6.25–100 µg/mL) of algal extract, CuO NPs, and starch/PVA/CuO nanoscaffolds in triplicates. Following 24 hours of incubation at 37°C in 5% CO_2, MTT reagent was added and incubated for 4 more hours. Formazan crystals were dissolved in 200 µL DMSO, and absorbance was measured at 570 nm using a spectrophotometer. Experiments were conducted in triplicate, and mean optical density (OD) with standard deviation was calculated for each treatment group [42].

2.8. Statistical analysis

All experimental outcomes were statistically evaluated using SPSS version 25.0 and GraphPad Prism version 9.0. Data from triplicate trials were expressed as mean ± standard deviation. One-way ANOVA was used to determine statistical differences among groups, followed by post-hoc tests such as Tukey's or Dunnett's where relevant. A p-value < 0.05 was deemed statistically significant. Correlations were analyzed using Pearson's coefficient. The Shapiro–Wilk test assessed normality; if violated, data underwent logarithmic transformation. All conclusions were drawn at a 95% confidence level to ensure robustness and reproducibility [43].

3. RESULTS

3.1. UV–visible spectroscopic characterization

The UV–Visible absorption spectra (Fig. 1) for the *Ectocarpales* extract and the synthesized CuO NPs were recorded using a JASCO UV-VIS spectrophotometer (Model V-730), scanning wavelengths from 200 to 800 nm. Deionized water was employed as the blank. The *Ectocarpales* extract demonstrated a broad absorption band spanning 200–400 nm, with a prominent peak near 300 nm exhibiting an absorbance value of 0.93687. This feature is characteristic of π-π* transitions, commonly linked to phenolic groups, flavonoids, and chlorophyll derivatives in marine algae. Absorbance steadily decreased from 400 to 800 nm, indicating minimal interaction within the visible range, consistent with the limited presence of extensive conjugated systems.

In contrast, the CuO NPs showed a distinct UV absorption edge with a sharp peak at 200 nm (absorbance: 0.53295), reflecting their intrinsic bandgap and possible surface plasmon resonance phenomena. Absorbance diminished gradually at longer wavelengths, a typical behavior of semiconducting nanoparticles. The notable differences between the extract and CuO NPs highlight their differing chemical nature—organic compounds in the extract versus inorganic nanoparticles. These spectra confirm the successful synthesis and distinct optical signatures of both samples.

3.2. FTIR spectral analysis

Fourier-transform infrared (FT-IR) spectra (Fig. 2) for the CuO NPs and the fabricated nanoscaffolds were obtained using a PerkinElmer Spectrum Two spectrometer equipped with Attenuated Total Reflectance (ATR) from 4000 to 400 cm^{-1}, at 4 cm^{-1} resolution and 64 scans. The CuO NPs displayed prominent absorption bands at 3216 cm^{-1}, attributed to O–H stretching due to adsorbed moisture, and at 1511 cm^{-1}, likely from C=O stretching or aromatic ring vibrations. A distinct peak at 860 cm^{-1} corresponded to Cu–O bond stretching, confirming copper oxide formation alongside residual organic moieties from synthesis.

The nanoscaffold spectrum exhibited broader, more complex bands with a strong peak at 3298 cm^{-1} assigned to O–H and/or N–H stretching common in polymeric materials. A band at 2107 cm^{-1} indicated C≡N or conjugated C=C=N functionalities. Peaks at 1652 cm^{-1} and 1327 cm^{-1} were related to C=O stretching and O–H or C–N bending, respectively. Additional bands at 840 cm^{-1} and 607 cm^{-1} suggested glycosidic linkages and inorganic-polymer interactions. These findings confirm CuO NP synthesis and their successful incorporation into the polymer scaffold matrix.

3.3. XRD analysis

X-ray diffraction (XRD) patterns (Fig. 3) of CuO NPs and nanoscaffolds were recorded using a Bruker D8 Advance diffractometer with CuKα radiation (λ = 1.5406 Å) operating at 40 kV and 40 mA. Data were collected over a 2θ range of 5° to 90°, with a step size of 0.029649°. The CuO NPs revealed 25 distinct diffraction peaks, with intense reflections at 26.201° (d = 3.398 Å), 20.312° (d = 4.369 Å), and 36.148° (d = 2.483 Å), matching the monoclinic tenorite phase (JCPDS No. 05-0661). The sharpness and narrow full-width half maximum (FWHM) confirmed high crystallinity.

Nanoscaffolds showed 14 diffraction peaks, dominated by signals at 21.199° (d = 4.188 Å) and 30.844° (d = 2.897 Å), indicative of a semi-crystalline polymeric matrix, calculated as 15.9% crystalline and 84.1% amorphous. The broadened peaks and larger FWHM suggested reduced structural order due to CuO NP dispersion within the polymer. No peak overlaps were observed, confirming the structural integrity and purity of both CuO NPs and nanoscaffolds.

3.4. SEM analysis

Scanning electron microscopy (SEM) images (Fig. 4), acquired using a JEOL JSM-IT800 NANO SEM, provided morphological characterization of the CuO NPs and nanofibrous scaffolds. The CuO NPs were mainly spherical to slightly irregular, with sizes ranging from 50 to 200 nm. Slight agglomeration was evident, possibly due to high surface energy, yet discrete particles were clearly discernible.

The nanoscaffolds revealed a porous, interconnected fibrous network with fiber diameters between 70 and 90 nm. Fibers exhibited smooth morphology with occasional bead formation, indicative of well-optimized electrospinning parameters. Bright spots visible on the fiber surfaces corresponded to embedded CuO NPs, confirming their uniform distribution within the scaffold. This hierarchical porous structure with well-incorporated NPs suggests excellent potential for biomedical uses, such as tissue engineering and wound healing, with minimal nanoparticle aggregation.

3.5. TGA

Thermogravimetric analysis (TGA) of the nanoscaffolds (Fig. 5) was performed using a PerkinElmer TGA 8000 instrument. A 1.012 mg sample was heated from ambient temperature to 600°C under nitrogen at 15°C/min. The thermogram showed a multi-step degradation pattern. An initial weight loss of 3.581% below 100°C was attributed to moisture and solvent evaporation. The main degradation occurred at 336.92°C, corresponding to polymer matrix decomposition (e.g., starch or PVA). Complete degradation finished by 400.84°C, leaving a residue of 31.102%, attributed to CuO NPs. The relatively high degradation temperature and significant residual mass highlight the scaffold's thermal stability, making it suitable for thermally demanding applications. These results confirm the robust composite nature and structural integrity of the nanoscaffold.

3.6. Dynamic light scattering (DLS) and zeta potential

DLS and zeta potential analyses were performed using a Malvern Zetasizer Ultra to determine the hydrodynamic size and surface charge of CuO NPs. The DLS revealed an average hydrodynamic diameter (Z-average) of 79.8 nm (Fig. 6) with a polydispersity index (PDI) of 0.475, indicating moderate size heterogeneity. The zeta potential

measurements (Fig. 7) showed an average surface charge of +14.03 mV, with two main populations at +10.94 mV and +28.06 mV. The positive charge is likely due to residual organic capping agents from the biogenic synthesis process.

The nanoparticle suspension had a conductivity of 0.1179 mS/cm and a quality factor of 2.084, indicating a relatively stable colloidal dispersion. Although some larger aggregates were present, the CuO NPs exhibited adequate dispersibility and surface charge stability, supporting their potential use in biomedical and environmental applications. These physical characteristics are critical for understanding NP interactions in colloidal systems.

3.7. Anticancer activity evaluation

The results demonstrated a dose-dependent reduction in cell viability for all tested compounds—algal extract, CuO NPs, and starch/PVA/CuO-NPs nanoscaffolds—in both HT-29 and MCF-7 cancer cell lines.

For HT-29 cells, the algal extract reduced cell viability from 100% (untreated control) to 31.05% at the highest tested concentration (100 µg/mL). The IC_{50}, representing the concentration required to inhibit 50% of cell growth, was approximately 35 µg/mL, indicating moderate anticancer activity. In comparison, CuO NPs exhibited stronger cytotoxicity, decreasing viability to 20.63% at 100 µg/mL, with an IC_{50} of 15 µg/mL. The most potent effect was observed with starch/PVA/CuO-NPs nanoscaffolds, which reduced viability to just 13.68% at 100 µg/mL, yielding an IC_{50} of 10 µg/mL. This suggests that the nanoscaffold formulation significantly enhances the anticancer efficacy compared to CuO NPs alone.

In MCF-7 cells, a similar trend was observed. The algal extract reduced viability from 100% to 44.85% at 100 µg/mL, with an IC_{50} of 40 µg/mL, confirming its weaker cytotoxic effect compared to the other formulations. CuO NPs demonstrated improved activity, lowering viability to 36.27% at the same concentration, with an IC_{50} of 30 µg/mL. Once again, the starch/PVA/CuO-NPs nanoscaffolds outperformed both the extract and CuO NPs, reducing viability to 23.22% at 100 µg/mL and achieving an IC_{50} of 20 µg/mL.

The findings highlight that starch/PVA/CuO-NPs nanoscaffolds exhibit the highest anticancer activity against both HT-29 and MCF-7 cell lines, as evidenced by their significantly lower IC_{50} values compared to CuO NPs and algal extract. While CuO NPs showed intermediate cytotoxicity, the algal extract was the least potent. These results underscore the potential of nanoscaffolds as an advanced therapeutic strategy for cancer treatment, likely due to enhanced drug delivery and bioavailability. Further research is warranted to elucidate the underlying mechanisms and validate these findings in *in vivo* models.

4. DISCUSSION

The comprehensive characterization of the *Ectocarpales* extract, synthesized CuO NPs, and their incorporation into starch/PVA nanoscaffolds revealed important insights into their physicochemical properties and anticancer potential. The UV–Visible spectroscopy analysis first highlighted distinct differences in optical behavior between the biogenic extract and the inorganic nanoparticles. The broad absorption band between 200 and 400 nm seen in the *Ectocarpales* extract aligns well with the presence of polyphenolic compounds such as flavonoids and chlorophyll derivatives, which are known for their bioactivity and antioxidant properties. These chromophores typically absorb in the UV range due to π-π* electronic transitions, validating the extract's rich organic composition. Conversely, the CuO NPs exhibited a sharp absorption edge at around 200 nm, characteristic of their intrinsic bandgap and semiconductor nature. The lack of significant absorption in the visible region further confirms their purity and absence of large conjugated organic molecules. This differentiation strongly supports the successful synthesis of inorganic CuO NPs distinctly separate from the biological constituents of the algae extract [44].

FTIR spectral analysis provided further molecular-level confirmation of the chemical structures involved. The CuO NPs displayed signature bands corresponding to Cu–O stretching vibrations, particularly the peak near 860 cm^{-1}, which is a hallmark of copper oxide formation. Simultaneously, the presence of O–H and C=O related bands suggests the persistence of surface-bound organic groups from the green synthesis method, which may serve as natural capping agents enhancing nanoparticle stability. When embedded in the starch/PVA matrix, the nanoscaffold's spectrum exhibited broader and more complex features. The dominant O–H and N–H stretching vibrations, alongside peaks attributable to polymer backbone functionalities such as C=O and glycosidic linkages, confirmed the successful integration of CuO NPs within a polymeric scaffold. The interaction between the inorganic nanoparticles and the polymer matrix likely induces subtle shifts in bond vibrations, reflecting a well-dispersed composite structure critical for stable and functional biomaterials [45, 46].

XRD patterns further elucidated the crystalline nature of the synthesized materials. The CuO NPs demonstrated multiple sharp peaks consistent with the monoclinic tenorite phase, indicating high crystallinity and phase purity. Such well-defined crystallinity is often correlated with enhanced physicochemical stability and predictable biological activity, which is crucial for therapeutic applications. In contrast, the nanoscaffolds exhibited a predominantly amorphous profile with fewer and broader peaks, characteristic of semi-crystalline polymers. The reduced crystallinity and peak broadening are expected outcomes when nanoparticles are homogeneously distributed within a polymeric network, which disrupts regular polymer packing. Importantly, the absence of overlapping peaks between CuO and the polymer matrix suggests the materials retain their individual structural identities without forming unintended phases, preserving the functional properties of both components [47].

Morphological examination via SEM revealed the spherical to slightly irregular shape of CuO NPs, with sizes ranging from approximately 50 to 200 nm. This size distribution aligns with DLS results and supports their nanoscale dimension, which is essential for effective cellular interaction and penetration. The observed mild agglomeration is typical for metal oxide nanoparticles due to their high surface energy but did not impede their clear visualization as discrete particles. In the nanoscaffold, the formation of a continuous, interconnected fibrous network with uniform fiber diameters between 70 and 90 nm was evident. The presence of bright spots attributed to embedded CuO NPs confirms their homogeneous dispersion within the scaffold fibers. This hierarchical porous structure mimics extracellular matrix architecture, promoting cell attachment, proliferation, and nutrient exchange, which are desirable features for biomedical applications such as wound healing or targeted drug delivery [48, 49].
TGA indicated that the nanoscaffold exhibited considerable thermal stability, with primary polymer decomposition occurring near 337°C and a substantial residual mass (~31%) attributed to the inorganic CuO content. The initial moisture loss under 100°C is typical and reflects bound water within the hydrophilic polymer matrix. The high degradation temperature and significant residue demonstrate the scaffold's robustness, an advantageous property for materials intended for biomedical devices that may encounter varying environmental and physiological temperatures during processing or application. Such thermal characteristics also suggest potential for sterilization processes, expanding their practical usability [48, 50, 51].
The physicochemical stability of CuO NPs in colloidal suspension was corroborated by DLS and zeta potential analyses. The moderately narrow size distribution with a polydispersity index below 0.5 and a positive surface charge of approximately +14 mV indicate reasonable colloidal stability, possibly stabilized by organic moieties from the green synthesis. A positive surface charge favors interaction with negatively charged biological membranes, enhancing cellular uptake. Moreover, the relatively low conductivity and quality factor values reflect an adequately stable dispersion, critical for maintaining bioactivity and minimizing aggregation during application [52, 53].
The anticancer evaluation against HT-29 (colon carcinoma) and MCF-7 (breast carcinoma) cell lines revealed a clear hierarchy in cytotoxic efficacy. The biogenic *Ectocarpales* extract displayed moderate anticancer activity, likely attributable to bioactive phytochemicals such as polyphenols and flavonoids, which have known antiproliferative effects. However, its potency was surpassed by the CuO NPs, which exerted stronger cytotoxic effects, consistent with the reported ability of metal oxide NPs to induce reactive oxygen species (ROS) generation and mitochondrial dysfunction in cancer cells. Most notably, the starch/PVA/CuO nanoscaffolds exhibited the highest anticancer efficacy with significantly lower IC_{50} values across both cell lines. This enhanced activity can be explained by the synergistic effect of the polymeric matrix facilitating sustained and targeted release of CuO NPs, improving bioavailability and cellular uptake, while potentially mitigating nonspecific toxicity. The nanoscaffold's porous structure may also promote direct interaction with cancer cells, further amplifying therapeutic outcomes. These results highlight the promise of polymer-nanoparticle composites as advanced platforms for anticancer drug delivery, combining biocompatibility, structural support, and controlled cytotoxicity [54, 55].
The findings of this study demonstrate that green-synthesized CuO NPs possess desirable physicochemical and biological properties for cancer therapy, which are significantly augmented when incorporated into starch/PVA nanoscaffolds. This composite material combines the benefits of natural polymer matrices with the potent anticancer activity of metal oxide nanoparticles, yielding a multifunctional scaffold with potential applications in targeted cancer treatment and tissue engineering. Future studies exploring *in vivo* efficacy, detailed mechanistic pathways, and long-term biocompatibility will be critical to fully realize their clinical potential.

5. CONCLUSION

This study successfully demonstrated the biosynthesis of CuO NPs using *Ectocarpales* extract, followed by their effective incorporation into starch/PVA-based nanoscaffolds. Comprehensive characterization through UV-Vis, FT-IR, XRD, SEM, TGA, and DLS confirmed the formation, structural integrity, and stability of the synthesized CuO NPs and their uniform distribution within the nanofibrous scaffold matrix. The nanoscaffolds exhibited enhanced thermal stability and a porous morphology favorable for biomedical applications. Importantly, the anticancer assays revealed that the starch/PVA/CuO-NPs nanoscaffolds exhibited superior cytotoxicity against HT-29 and MCF-7 cancer cell lines compared to CuO NPs and algal extract alone, indicating synergistic effects likely due to improved nanoparticle delivery and interaction with cancer cells. These findings suggest that the developed nanoscaffolds hold significant promise as efficient anticancer agents, paving the way for further in-depth mechanistic studies and potential *in vivo* evaluations to advance their clinical applicability.
Data Availability Statement: The full dataset of physiochemical characterization associated with this work is published in Mendeley Data (doi: 10.17632/m7jzmb7mr9.1). **Disclosure:** The material characterization data and figures (e.g., UV, SEM, FTIR, XRD, TGA, Zeta Potential and particle sizer) presented here were generated from a common dataset and are being reused across multiple related studies on nanomaterials. All biological and environmental analyses and conclusions are original to each manuscript.

Conflicts of Interest: The authors declare no conflicts of interest.

REFERENCES

[1] A. Zafar, S. Khatoon, M.J. Khan, J. Abu, A. Naeem, Advancements and limitations in traditional anti-cancer therapies: a comprehensive review of surgery, chemotherapy, radiation therapy, and hormonal therapy, Discover Oncology, 16 (2025) 607.
[2] S.S. Dhilip Kumar, H. Abrahamse, Recent advances in the development of biocompatible nanocarriers and their cancer cell targeting efficiency in photodynamic therapy, Frontiers in chemistry, 10 (2022) 969809.
[3] T. Sahu, Y.K. Ratre, S. Chauhan, L. Bhaskar, M.P. Nair, H.K. Verma, Nanotechnology based drug delivery system: Current strategies and emerging therapeutic potential for medical science, Journal of Drug Delivery Science and Technology, 63 (2021) 102487.
[4] M.T. Yassin, F.O. Al-Otibi, S.A. Al-Sahli, M.S. El-Wetidy, S. Mohamed, Metal Oxide Nanoparticles as Efficient Nanocarriers for Targeted Cancer Therapy: Addressing Chemotherapy-Induced Disabilities, Cancers, 16 (2024) 4234.
[5] M.H. Saleem, U. Ejaz, M. Vithanage, N. Bolan, K.H. Siddique, Synthesis, characterization, and advanced sustainable applications of copper oxide nanoparticles: a review, Clean Technologies and Environmental Policy, (2024) 1-26.
[6] M. Ahamed, R. Lateef, M.J. Akhtar, P. Rajanahalli, Dietary antioxidant curcumin mitigates CuO nanoparticle-induced cytotoxicity through the oxidative stress pathway in human placental cells, Molecules, 27 (2022) 7378.
[7] D. Gupta, A. Boora, A. Thakur, T.K. Gupta, Green and sustainable synthesis of nanomaterials: recent advancements and limitations, Environmental Research, 231 (2023) 116316.
[8] S. Mahmood Ansari, Q. Saquib, V. De Matteis, H. Awad Alwathnani, S. Ali Alharbi, A. Ali Al-Khedhairy, Marine macroalgae display bioreductant efficacy for fabricating metallic nanoparticles: intra/extracellular mechanism and potential biomedical applications, Bioinorg. Chem. Appl., 2021 (2021) 5985377.
[9] V. Lemesheva, R. Islamova, E. Stepchenkova, A. Shenfeld, C. Birkemeyer, E. Tarakhovskaya, Antibacterial, antifungal and algicidal activity of phlorotannins, as principal biologically active components of ten species of brown algae, Plants, 12 (2023) 821.
[10] N. Ahmed, M.A. Sheikh, M. Ubaid, P. Chauhan, K. Kumar, S. Choudhary, Comprehensive exploration of marine algae diversity, bioactive compounds, health benefits, regulatory issues, and food and drug applications, Measurement: Food, (2024) 100163.
[11] A. Mounika, B. Ilangovan, S. Mandal, W.S. Yashwant, S.P. Gali, A. Shanmugam, Prospects of ultrasonically extracted food bioactives in the field of non-invasive biomedical applications–A review, Ultrasonics Sonochemistry, 89 (2022) 106121.
[12] J. Liang, P. Liu, X. Yang, L. Liu, Y. Zhang, Q. Wang, H. Zhao, Biomaterial-based scaffolds in promotion of cartilage regeneration: recent advances and emerging applications, Journal of Orthopaedic Translation, 41 (2023) 54-62.
[13] E. Ahmadian, A. Eftekhari, D. Janas, P. Vahedi, Nanofiber scaffolds based on extracellular matrix for articular cartilage engineering: a perspective, Nanotheranostics, 7 (2023) 61.
[14] X. Bai, Z.L. Smith, Y. Wang, S. Butterworth, A. Tirella, Sustained drug release from smart nanoparticles in cancer therapy: a comprehensive review, Micromachines, 13 (2022) 1623.
[15] X. Liang, H.-J. Zhong, H. Ding, B. Yu, X. Ma, X. Liu, C.-M. Chong, J. He, Polyvinyl alcohol (PVA)-based hydrogels: Recent progress in fabrication, properties, and multifunctional applications, Polymers, 16 (2024) 2755.
[16] A.S. Elgharbawy, A.-G.M. El Demerdash, W.A. Sadik, M.A. Kasaby, A.H. Lotfy, A.I. Osman, Synthetic degradable polyvinyl alcohol polymer and its blends with starch and cellulose—A comprehensive overview, Polymers, 16 (2024) 1356.
[17] S. Patil, A.K. Bharimalla, A. Mahapatra, J. Dhakane-Lad, A. Arputharaj, M. Kumar, A. Raja, N. Kambli, Effect of polymer blending on mechanical and barrier properties of starch-polyvinyl alcohol based biodegradable composite films, Food Bioscience, 44 (2021) 101352.
[18] I.R.S. Vieira, A.P.A.d. de Carvalho, C.A. Conte-Junior, Recent advances in biobased and biodegradable polymer nanocomposites, nanoparticles, and natural antioxidants for antibacterial and antioxidant food packaging applications, Comprehensive reviews in food science and food safety, 21 (2022) 3673-3716.
[19] N. Yosri, S.A. Khalifa, N.F. Attia, M. Du, L. Yin, T.Z. Abolibda, K. Zhai, Z. Guo, H.R. El-Seedi, Advancing sustainability in the green engineering of nanocomposites based on marine-derived polymers and their applications: A comprehensive review, International Journal of Biological Macromolecules, (2024) 133249.
[20] L. Li, R. Hao, J. Qin, J. Song, X. Chen, F. Rao, J. Zhai, Y. Zhao, L. Zhang, J. Xue, Electrospun fibers control drug delivery for tissue regeneration and cancer therapy, Advanced Fiber Materials, 4 (2022) 1375-1413.
[21] M.E. Astaneh, N. Fereydouni, Electrospun-based nanofibers as ROS-scavenging scaffolds for accelerated wound healing: a narrative review, International Journal of Polymeric Materials and Polymeric Biomaterials, (2024) 1-33.
[22] A.A. Badawy, N.A. Abdelfattah, S.S. Salem, M.F. Awad, A. Fouda, Efficacy assessment of biosynthesized copper oxide nanoparticles (CuO-NPs) on stored grain insects and their impacts on morphological and physiological traits of wheat (Triticum aestivum L.) plant, Biology, 10 (2021) 233.
[23] B. Uzair, N. Syed, A. Kanwal, G. Samin, M.B.K. Niazi, S. Abbas, A.S. Alotaibi, H. Ghabban, A.E. Albalawi, N. Alsowayeh, Synthesis of AgO/CuO/PVA/starch hydrogel by casting method and characterizations to safely

overcome skin infections: A possible application in wound healing as a dressing, Materials Today Communications, 39 (2024) 109286.
[24] N. Hazhir, F. Chekin, J.B. Raoof, S. Fathi, Anticancer activity of Doxorubicin conjugated to polymer/carbon based-nanohybrid against MCF-7 breast and HT-29 colon cancer cells, International Journal of Nano Dimension, 12 (2021).
[25] A. Kumar, Y. Rai, A.N. Bhatt, Anti-cancer drug-mediated increase in mitochondrial mass limits the application of metabolic viability-based MTT assay in cytotoxicity screening, Cytotechnology, 76 (2024) 301-311.
[26] Z. Yu, M. Guindani, S.F. Grieco, L. Chen, T.C. Holmes, X. Xu, Beyond t test and ANOVA: applications of mixed-effects models for more rigorous statistical analysis in neuroscience research, Neuron, 110 (2022) 21-35.
[27] J. Indrakumar, S. Sankar, H. Madhyastha, G.K. Muthukaliannan, Progressive application of marine biomaterials in targeted cancer nanotherapeutics, Current Pharmaceutical Design, 28 (2022) 3337-3350.
[28] T. Saini, J. Meena, V. Verma, S. Saini, R. Malik, Polyvinyl Alcohol: Recent Advances and Applications in Sustainable Materials, Polymer-Plastics Technology and Materials, (2025) 1-32.
[29] S.S. Shahriar, S.M. Andrabi, F. Islam, J.M. An, S.J. Schindler, M.P. Matis, D.Y. Lee, Y.-k. Lee, Next-generation 3D scaffolds for nano-based chemotherapeutics delivery and cancer treatment, Pharmaceutics, 14 (2022) 2712.
[30] R. Martins, C. Mouro, R. Pontes, J. Nunes, I. Gouveia, Ultrasound-assisted extraction of bioactive pigments from Spirulina platensis in natural deep eutectic solvents, Bioresources and Bioprocessing, 10 (2023) 88.
[31] A. Martín-del-Campo, J.A. Fermín-Jiménez, V.V. Fernández-Escamilla, Z.Y. Escalante-García, M.E. Macías-Rodríguez, Y. Estrada-Girón, Improved extraction of carrageenan from red seaweed (Chondracantus canaliculatus) using ultrasound-assisted methods and evaluation of the yield, physicochemical properties and functional groups, Food Science and Biotechnology, 30 (2021) 901-910.
[32] G. Anbalagan, B. Subramanian, V. Suresh, P. Sivaperumal, Green synthesis of copper and copper oxide nanoparticles from brown algae turbinaria species' aqueous extract and its antibacterial properties, Cureus, 16 (2024).
[33] A. Filimon, A.M. Dobos, M.D. Onofrei, D. Serbezeanu, Polyvinyl Alcohol-Based Membranes: A Review of Research Progress on Design and Predictive Modeling of Properties for Targeted Application, Polymers, 17 (2025) 1016.
[34] A.L. Sunarwidhi, A. Hernawan, A. Frediansyah, S. Widyastuti, N.W.R. Martyasari, A.S. Abidin, H. Padmi, E. Handayani, N.W.P. Utami, F.A. Maulana, Multivariate analysis revealed ultrasonic-assisted extraction improves anti-melanoma activity of non-flavonoid compounds in indonesian brown algae ethanol extract, Molecules, 27 (2022) 7509.
[35] M.M. Rahman Khan, M.M.H. Rumon, M. Islam, Synthesis, Rheology, Morphology, and Mechanical Properties of Biodegradable PVA-Based Composite Films: A Review on Recent Progress, Processes, 12 (2024).
[36] G. Ateş, S. Bilici, Investigation of spectral and optical properties of some organic eyeglass lenses, İnönü Üniversitesi Sağlık Hizmetleri Meslek Yüksek Okulu Dergisi, 11 (2023) 1042-1053.
[37] P. Meyvisch, P.R. Gurdebeke, H. Vrielinck, K. Neil Mertens, G. Versteegh, S. Louwye, Attenuated Total reflection (ATR) Micro-Fourier transform infrared (Micro-FT-IR) spectroscopy to enhance repeatability and reproducibility of spectra derived from single specimen organic-walled dinoflagellate cysts, Applied Spectroscopy, 76 (2022) 235-254.
[38] M. Aslam, M.A. Kalyar, Z.A. Raza, Fabrication of nano-CuO-loaded PVA composite films with enhanced optomechanical properties, Polymer Bulletin, 78 (2021) 1551-1571.
[39] H. Ullah, F. Usman, M.A. Rasheed, A.A. Khan, R. Ahmad, S.Y. Lee, J. Heo, G. Ali, M. Khan, S.O. Cho, Anodic SnO2 nanoporous channels functionalized with CuO quantum dots for selective H2O2 biosensing, ACS Applied Nano Materials, 5 (2022) 9096-9111.
[40] P. Safari, E.Z. Rahimabadi, M.R. Vaezi, A. Behnamghader, R. Tahergorabi, Development of ZnO-NPs reinforced chitosan nanofiber mats with improved antibacterial and biocompatibility properties, Sci Rep, 15 (2025) 1-17.
[41] M.B. Mobarak, M.S. Hossain, F. Chowdhury, S. Ahmed, Synthesis and characterization of CuO nanoparticles utilizing waste fish scale and exploitation of XRD peak profile analysis for approximating the structural parameters, Arabian Journal of Chemistry, 15 (2022) 104117.
[42] D. Duarte, A. Cardoso, N. Vale, Synergistic growth inhibition of HT-29 colon and MCF-7 breast cancer cells with simultaneous and sequential combinations of antineoplastics and CNS drugs, International Journal of Molecular Sciences, 22 (2021) 7408.
[43] İ. Gulcin, S.H. Alwasel, DPPH radical scavenging assay, Processes, 11 (2023) 2248.
[44] M. Priya, R. Venkatesan, S. Deepa, S.S. Sana, S. Arumugam, A.M. Karami, A.A. Vetcher, S.-C. Kim, Green synthesis, characterization, antibacterial, and antifungal activity of copper oxide nanoparticles derived from Morinda citrifolia leaf extract, Sci Rep, 13 (2023) 18838.
[45] A.B.D. Nandiyanto, R. Ragadhita, M. Fiandini, Interpretation of Fourier transform infrared spectra (FTIR): A practical approach in the polymer/plastic thermal decomposition, Indonesian Journal of Science and Technology, 8 (2023) 113-126.

[46] S. Pasieczna-Patkowska, M. Cichy, J. Flieger, Application of Fourier Transform Infrared (FTIR) Spectroscopy in Characterization of Green Synthesized Nanoparticles, Molecules, 30 (2025) 684.
[47] R. Badry, M.M. El-Nahass, N. Nada, H. Elhaes, M.A. Ibrahim, Structural and UV-blocking properties of carboxymethyl cellulose sodium/CuO nanocomposite films, Sci Rep, 13 (2023) 1123.
[48] T.D.H. Le, H.N.A. Tuan, V.T. Nguyen, A.T. Le, Hydroxyapatite− loaded starch/polyvinyl alcohol scaffold for bone regeneration application: preparation and characterization, Journal of Sol-Gel Science and Technology, 107 (2023) 441-451.
[49] V. Harish, D. Tewari, M. Gaur, A.B. Yadav, S. Swaroop, M. Bechelany, A. Barhoum, Review on nanoparticles and nanostructured materials: Bioimaging, biosensing, drug delivery, tissue engineering, antimicrobial, and agro-food applications, Nanomaterials, 12 (2022) 457.
[50] S. Chandel, P. Pandey, S. Saini, R. Sharma, B. Parashar, K. Yadav, Natural Product-Loaded PCL and PLA-Based Bio-Scaffold and Their Applications, Natural Product Inspired Scaffolds: Applications in Tissue Engineering, Springer2024, pp. 117-146.
[51] M. Ramezani, Z.M. Ripin, An overview of enhancing the performance of medical implants with nanocomposites, Journal of Composites Science, 7 (2023) 199.
[52] S. Kamble, S. Agrawal, S. Cherumukkil, V. Sharma, R.V. Jasra, P. Munshi, Revisiting zeta potential, the key feature of interfacial phenomena, with applications and recent advancements, ChemistrySelect, 7 (2022) e202103084.
[53] A. Gordillo-Galeano, C.E. Mora-Huertas, Hydrodynamic diameter and zeta potential of nanostructured lipid carriers: Emphasizing some parameters for correct measurements, Colloids and surfaces A: Physicochemical and engineering aspects, 620 (2021) 126610.
[54] D.S. Bharathi, A. Boopathyraja, S. Nachimuthu, K. Kannan, Green Synthesis, Characterization and antibacterial activity of SiO 2–ZnO nanocomposite by Dictyota bartayresiana extract and its cytotoxic effect on HT29 Cell Line, Journal of Cluster Science, (2022) 1-17.
[55] S.H. El-Moslamy, Y.A. El-Maradny, M.H. El-Sayed, M.A. El-Sakhawy, E.M. El-Fakharany, Facile phyto-mediated synthesis of ternary CuO/Mn3O4/ZnO nanocomposite using Nigella Sativa seeds extract: characterization, antimicrobial, and biomedical evaluations, Sci Rep, 15 (2025) 1-21.

Figures

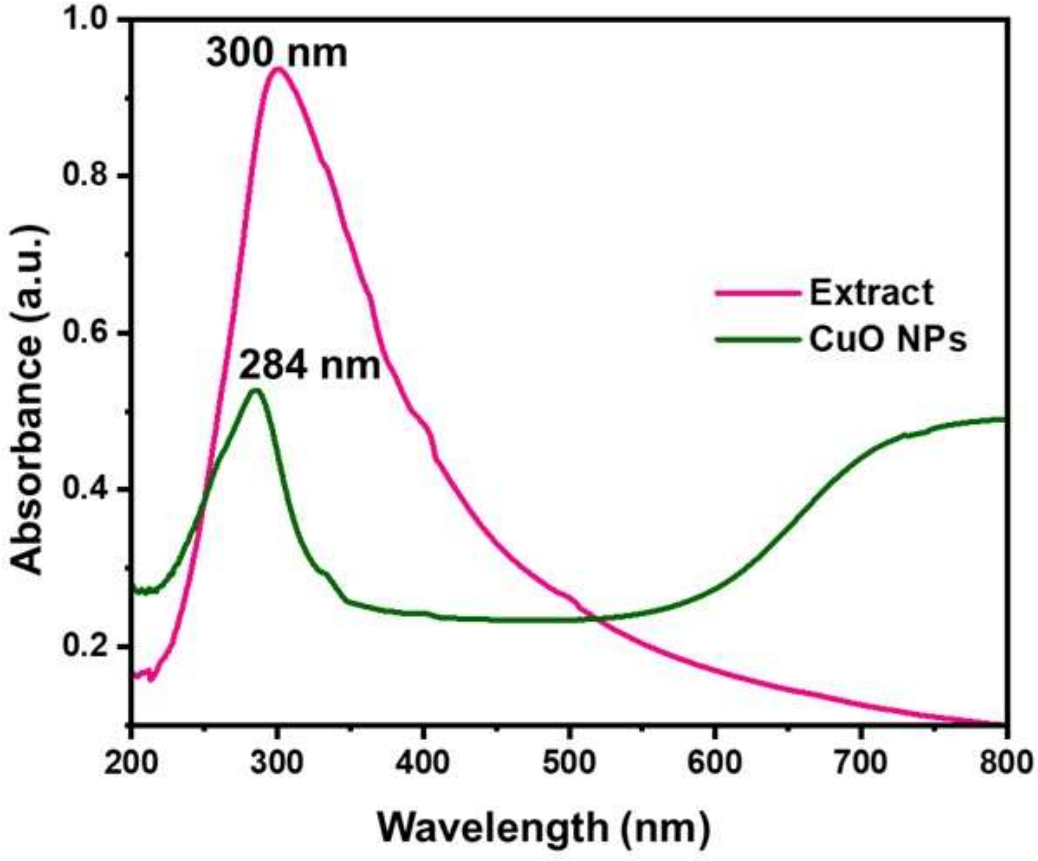

Fig. 1. UV–Visible Spectroscopy analysis of algae extract and CuO NPs

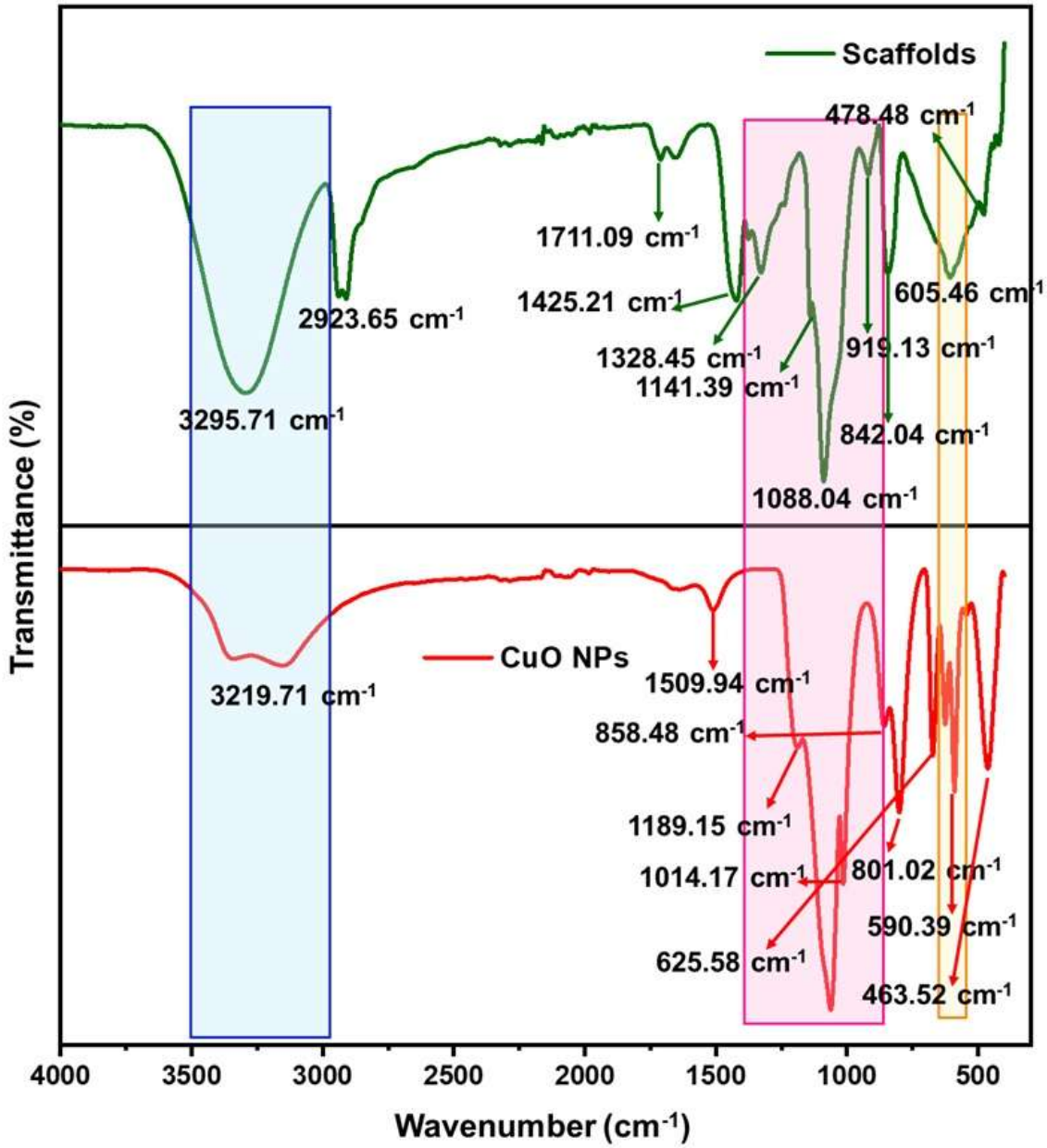

Fig. 2. FTIR analysis of CuO NPs and starch/PVA/CuONPs nanoscaffolds

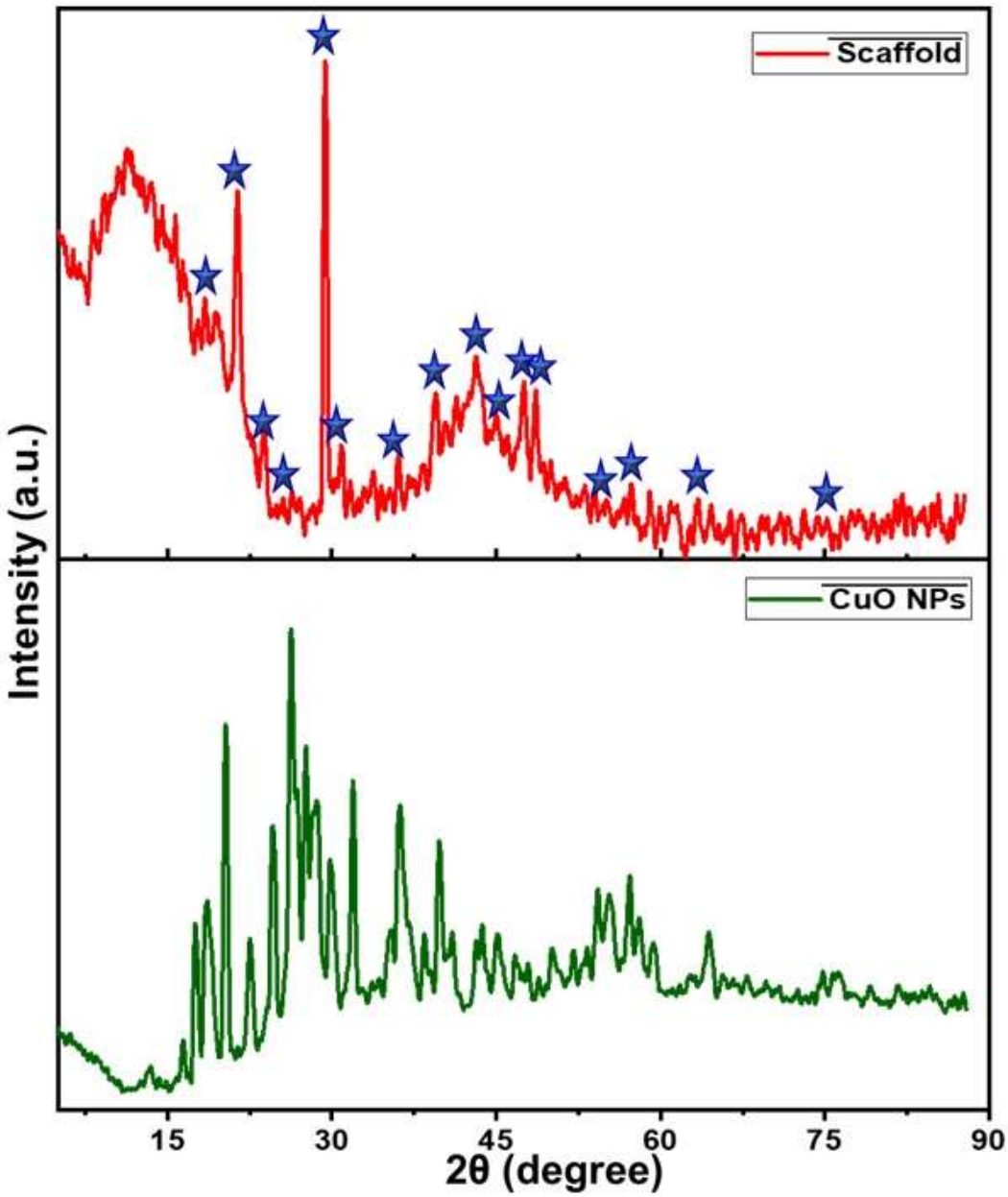

Fig. 3. XRD analysis of CuO NPs and starch/PVA/CuONPs nanoscaffolds

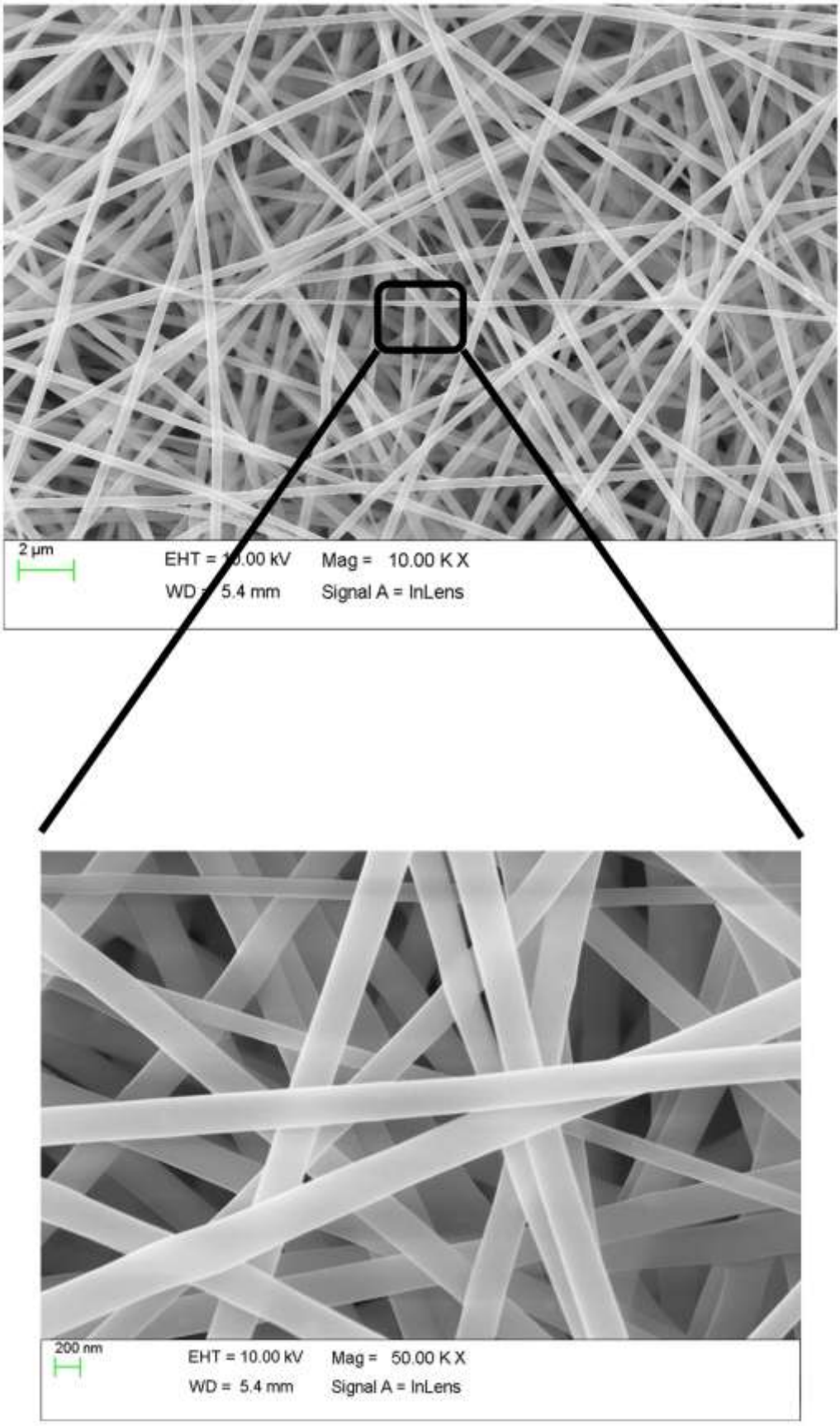

Fig. 4. SEM analysis of starch/PVA/CuONPs nanoscaffolds

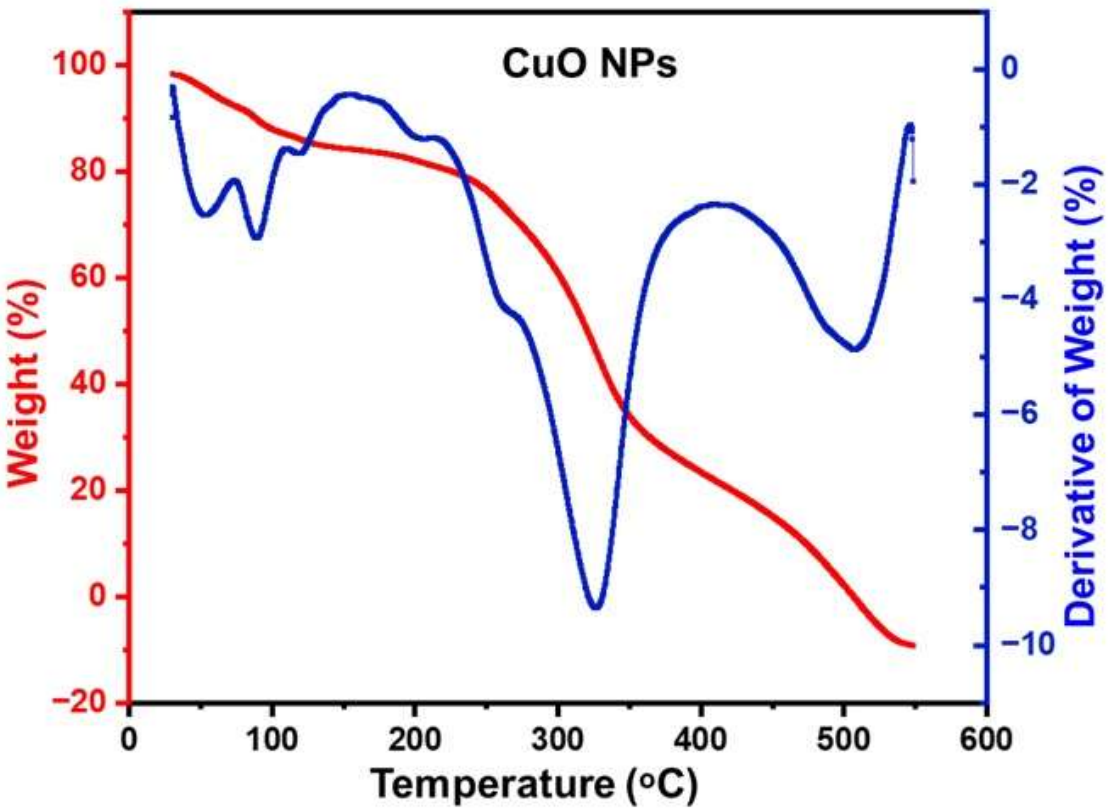

Fig. 5. TGA analysis of starch/PVA/CuONPs nanoscaffolds

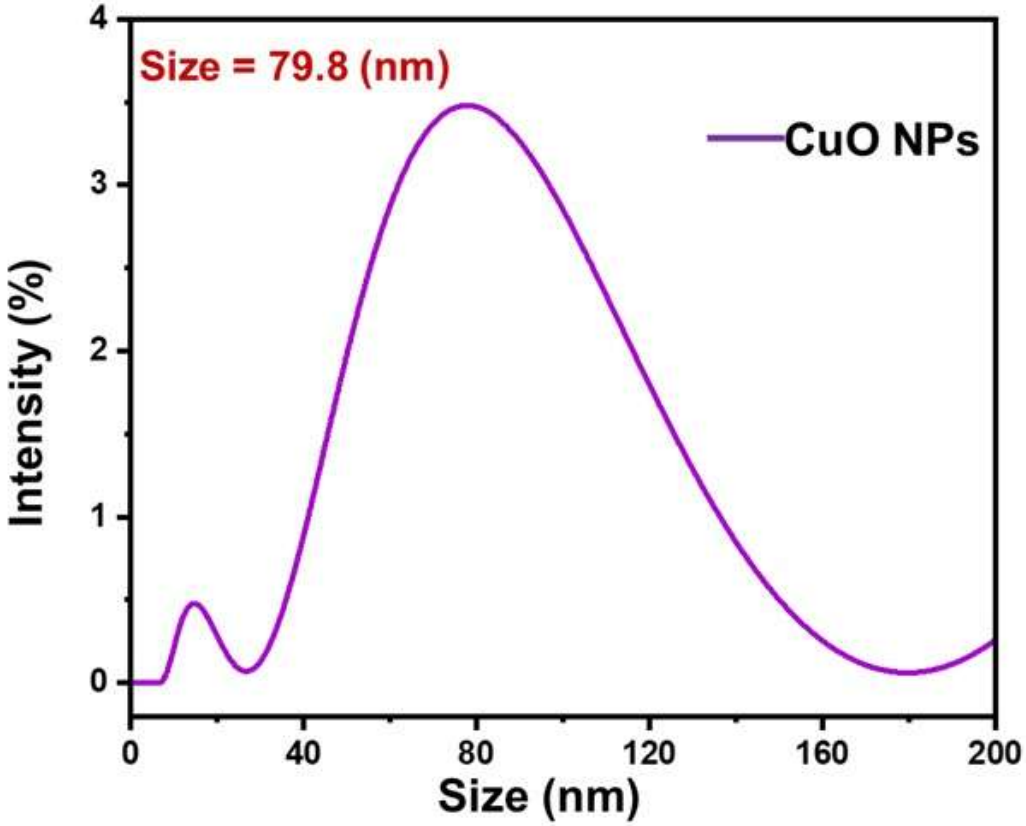

Fig. 6. Particle size analysis of CuO NPs

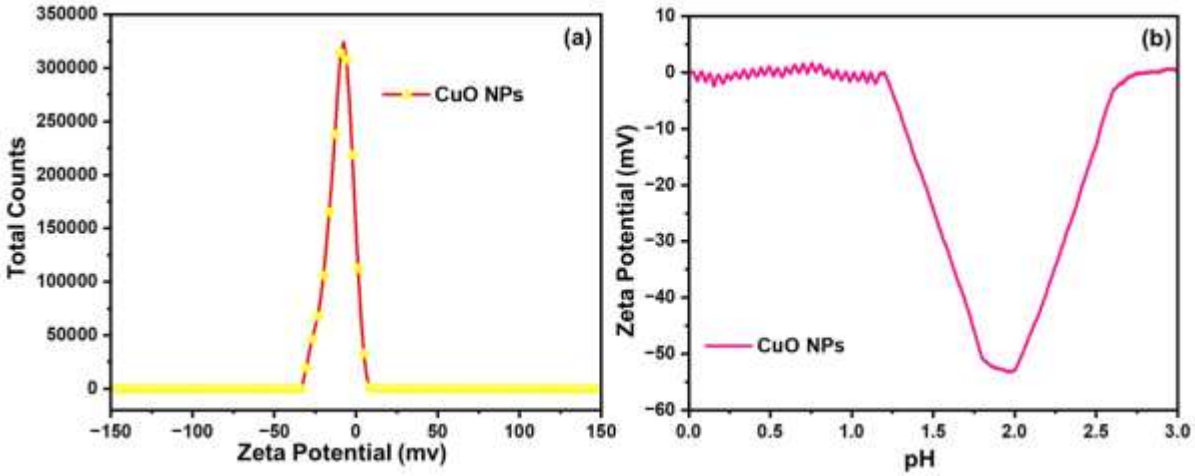

Fig. 7. Zeta potential analysis of CuO NPs

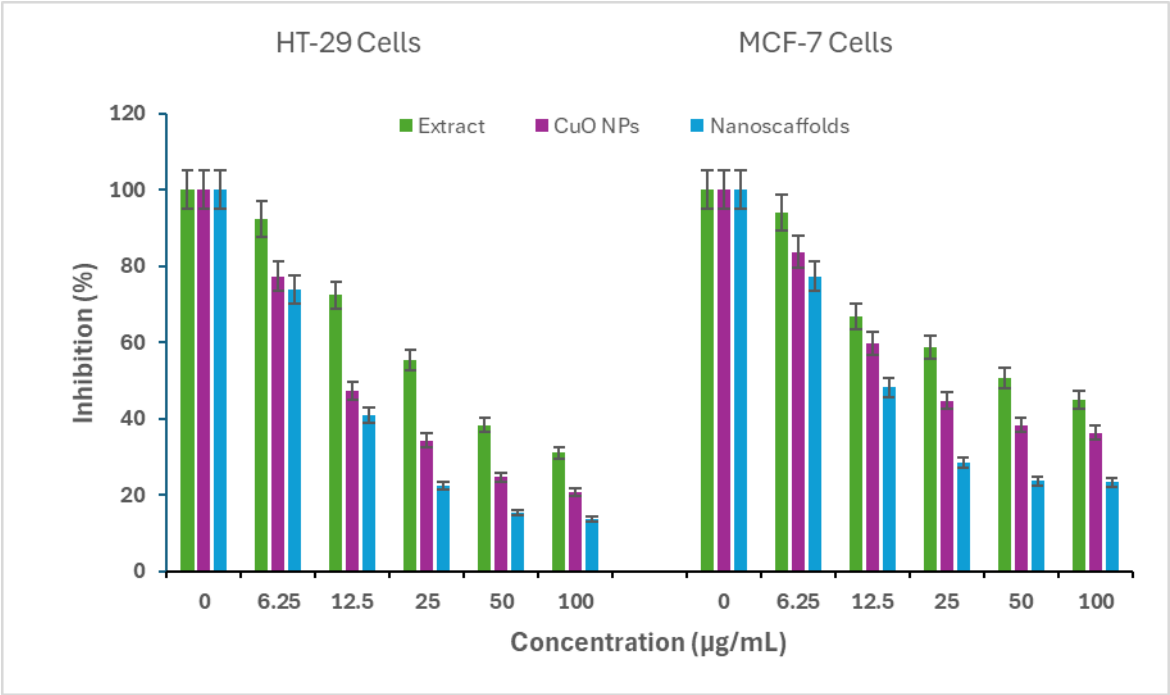

Fig. 8. Anticancer potential of algal extract, CuO NPs and starch/PVA/CuO-NPs nanoscaffolds